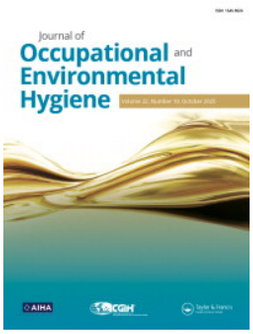

Taylor & Francis
Taylor & Francis Group

Journal of Occupational and Environmental Hygiene

ISSN: 1545-9624 (Print) 1545-9632 (Online) Journal homepage: www.tandfonline.com/journals/uoeh20

Computational modeling for PPE filtration: Informed by material characterization, microbial penetration, and particle mechanics

William Kastor, Andrew Martin, Sang Hyuk Lee, Xiao Fu, F. Selcen Kilinc-Balci, Christian Coby, Ethan Cohen, David M. Saylor, Robert Elder, Katherine Vorvolakos, Marc Donohue, Steven C. Wood & Enusha Karunasena

To cite this article: William Kastor, Andrew Martin, Sang Hyuk Lee, Xiao Fu, F. Selcen Kilinc-Balci, Christian Coby, Ethan Cohen, David M. Saylor, Robert Elder, Katherine Vorvolakos, Marc Donohue, Steven C. Wood & Enusha Karunasena (2025) Computational modeling for PPE filtration: Informed by material characterization, microbial penetration, and particle mechanics, Journal of Occupational and Environmental Hygiene, 22:10, 836-853, DOI: 10.1080/15459624.2025.2499611

To link to this article: https://doi.org/10.1080/15459624.2025.2499611

JOURNAL OF OCCUPATIONAL AND ENVIRONMENTAL HYGIENE
2025, VOL. 22, NO. 10, 836–853
https://doi.org/10.1080/15459624.2025.2499611

Computational modeling for PPE filtration: Informed by material characterization, microbial penetration, and particle mechanics

William Kastor[a,b]*, Andrew Martin[a,b]*, Sang Hyuk Lee[a,b,c]*, Xiao Fu[a], F. Selcen Kilinc-Balci[d], Christian Coby[d], Ethan Cohen[e], David M. Saylor[a], Robert Elder[a], Katherine Vorvolakos[a], Marc Donohue[c], Steven C. Wood[a], and Enusha Karunasena[a]

[a]Division of Biology, Chemistry, and Materials Science, Office of Science and Engineering Laboratories, US Food and Drug Administration (FDA), Oak Ridge, Tennessee; [b]Oak Ridge Institute for Science and Education Office of Science, US Department of Energy, Oak Ridge, Tennessee; [c]Department of Chemical and Biomolecular Engineering, Whiting School of Engineering, Johns Hopkins University, Baltimore, Maryland; [d]National Personal Protective Technology Laboratory, National Institute for Occupational Safety and Health, Centers for Disease Control and Prevention, Pittsburgh, Pennsylvania; [e]Division of Biological Physics, Office of Science and Engineering Laboratories, Center for Devices and Radiological Health, US Food and Drug Administration (FDA), Silver Spring, Maryland

ABSTRACT

This work assesses the current characterization framework of single-use personal protective equipment (PPE) per recognized consensus standards and presents a novel quantitative approach to refining characterization of barrier materials and predicting PPE performance. Scanning electron microscopy (SEM) and image analysis software (Diameter J) were used to examine the microscopic fiber and pore structure of filter layers of surgical N95 filtering facepiece respirators, before and after exposure to chemicals used in decontamination modalities (vaporized hydrogen peroxide or ozone). The effect of porosity on penetration was assessed by bacterial filtration efficiency (BFE) testing. Results from these experiments were incorporated into a physics-based computational model of overall filtration efficiency (OFE). Material thickness, fiber thickness, and packing density were introduced as inputs into a sequence of mathematical expressions to calculate OFE for filtration layers from surgical N95 respirators. OFE derived from the computational model was compared with experimental data for *Staphylococcus aureus* filtration (per ASTM F2101-23). The resulting output from the model is conservative and predictive when compared with experimental results to assess OFE and filtration efficiency relative to specific particle-size ranges. The model functions may be used to help inform or expedite design or manufacturing decision-making on surgical N95 respirators.

KEYWORDS

COVID; mask; N95; PPE; SARS; decontamination

Introduction

The COVID-19 pandemic was driven by the many variants of severe acute respiratory syndrome coronavirus 2 (SARS-CoV-2), which originated from Wuhan City in the Hubei Province of China in December 2019 (Hu et al. 2021). The World Health Organization (WHO) (2021) COVID-19 case tracker (Worldometer; https://www.worldometers.info/coronavirus/) reported on March 7, 2024, that the pandemic resulted in 700 million cases with 7 million deaths. In the U.S., there were approximately 111 million cases, with 1.2 million deaths.

Due to the virus's highly contagious nature, respiratory protective devices (e.g., N95 respirators), frequent handwashing, and use of disposable gowns, face shields, and gloves were needed to protect against its transmission (Hu et al. 2021). Real-world analysis following SARS-like events showed reductions in viral transmission with the use of PPE (reductions were reported at rates of 68% with masks, 91% with N95 respirators, 77% with gowns, and 57% with gloves), along with other methods (handwashing 10x daily), together decreased transmission by 55% (Adanur and Jayswal 2022; Jefferson et al. 2009).

CONTACT Enusha Karunasena Enusha.Karunasena@fda.hhs.gov Division of Biology, Chemistry, and Materials Science, Office of Science and Engineering Laboratories, US Food and Drug Administration (FDA), Oak Ridge, Tennessee.
*These authors contributed equally.

Supplemental data for this article can be accessed online at https://doi.org/10.1080/15459624.2025.2499611. AIHA and ACGIH members may also access supplementary material at http://oeh.tandfonline.com.

Surgical N95 filtering facepiece respirators (FFRs) are commonly used in healthcare settings. These devices are N95 FFRs approved by NIOSH as meeting the respiratory protection requirements of 42 C.F.R. Part 84. Worn by healthcare personnel to protect both the patient and the healthcare personnel from the transfer of microorganisms, body fluids, and particulates at an N95 filtration efficiency, they additionally conform to recognized standards for biocompatibility, flammability, and fluid resistance. These respirators filter out at least 95% of particles in the air, including large and small particles (10 µm–0.1 µm) if the respirator is properly fitted; however, improperly fitted respirators can significantly reduce PPE performance (Lawrence et al. 2006; Lin et al. 2021; National Institute for Occupational Safety and Health SB 2020).

The onset of the pandemic and the resulting global demand for PPE resulted in unprecedented demand (Chaib 2020; Cohen and Rodgers 2020). In 2020, estimated PPE for medical personnel alone was 89 million masks per month (Chaib 2020). Through national surveys in the U.S., 87% of nurses reported having to re-use single-use, disposable masks, and 27% reused disposable FFRs (Check et al. 2021; Cohen and Rodgers 2020).

As single-use disposables, most PPE, including gowns, gloves, surgical masks, and respirators, have been minimally studied for physics-based modeling (Hu et al. 2021; Masandawa et al. 2021). Therefore, there is both a need and an opportunity to examine single-use PPE with more quantitative methods with the intent of providing more precision in the information available to stakeholders involved in PPE manufacturing and testing (Bai et al. 2021; Hu et al. 2021). Needs in this area include technologies that support reuse of single-use PPE, along with decontamination modalities such as those that use vaporized hydrogen peroxide, ozone, UV, steam sterilization, microwaves, methylene blue treatment, and combinations of these technologies (Lendvay et al. 2022).

There is a wide range of barrier fabric types used in PPE, including nonwoven webs, woven fabrics, knitted fabrics, and aluminized laminates, among others (Dolez et al. 2022; Lou et al. 2021). In the current work, the focus was on the respective barrier fabrics of four de-identified commercially available surgical N95 respirators and compared these to a disposable face mask.

Reviewed and assessed in this current characterization, per relevant testing standards, are surgical N95 respirators (Rahman et al. 2022). This assessment included identifying limitations of the current framework that could be improved or refined, thus motivating the current study. Presented in this study is a novel characterization protocol using SEM, and results from standard Bacterial Filtration Efficiency (BFE) testing were employed. The combination informs a computational approach from well-established transport phenomena to yield a conservative performance model that is stratified along particle size ranges. The effect of chemical decontamination modalities on the physical properties of the barrier material is assessed using SEM and BFE and used to inform the model. The model is accessible on a web-based graphic user interface (GUI) and may be used to inform and expedite decisions around the design, manufacture, and potential use of surgical N95 respirators. A compendium of SEM images of surgical N95 respirators, along with Levels 3 and 4 surgical gowns and their quantitative physical characterization, is described in American Standards for Testing and Materials (ANSI/AAMI 2012).

Recognized standards for mask or respirator performance testing

Innovation focused on PPE development resulted in wider acknowledgment of recognized consensus standards to evaluate PPE performance and novel scientific tools to obviate some testing (Avinash Patil et al. 2022; Check et al. 2021; Lendvay et al. 2022; Rahman et al. 2022). Examples include the American Society for Testing and Materials International (ASTM) and the International Organization for Standardization (ISO). Recognition of standards by regulatory bodies, including these, ensures that protocols follow defined paths and the evaluation of data quality.

NIOSH evaluates particulate filtering respirators using a worst-case method (TEB-APR-STP-0059), exposing N95s to charge-neutralized NaCl aerosol (CMB 0.075 ± 0.02 µm, GSD < 1.86) at 85 L/min to approximate MPPS conditions (~0.050 µm for N-type respirators). A surgical N95 FFR offers the protection of both an N95 respirator and a surgical mask as a physical barrier to larger droplets. These respirators require testing for fluid resistance, biocompatibility, and flammability properties in addition to N95 filtration efficiency and inhalation and exhalation resistance requirements, Medical masks are commonly tested for bacterial filtration efficiency, differential pressure, submicron filtration efficiency, fluid resistance, and flammability per ASTM F2100-23 Standard for Performance of Materials Used in Medical Face Masks, summarized in Table 1.

Table 1. Classification of barrier performance of masks (Redrawn from ASTM 2100-23).

Barrier level	Bacterial Filtration Efficiency (BFE), %	Differential pressure, mmH_2O/cm^2	Sub-micron particulate filtration efficiency, %	Resistance to penetration by synthetic blood, minimum pressure in mm Hg for pass result	Flame spread
1	≥95	<5.0	≥80	80	Class 1
2	≥98	<6.0	≥85	120	Class 1
3	≥98	<6.0	≥85	160	Class 1

ASTM F2101-23, the standard test method for evaluating the BFE of medical face mask materials using a biological aerosol of *Staphylococcus aureus*, is one of the required test methods to assess the penetration properties of protective devices against large droplets. It is also a method for assessing surgical N95 clearance through the FDA. Barrier function of materials can be evaluated and quantified using this standard test method that analyzes the penetration of aerosolized *S. aureus* with a mean droplet size of 3.0 μM +/- 0.3 μM (though the microorganism is ∼1.2 μm). The advantage of the method is its reproducibility, robustness, and sensitivity. The method has been in use for many years, but it is not a high-throughput assay and requires specialized, expensive equipment and microbiology expertise to obtain reproducible results.

While the long-established rubric comprising the consensus standards described above provides valuable information, its labor-intensive and complex nature compels the creation of tools to inform and expedite decision-making. For example, the ability to expedite and narrow material options could prevent testing of poorly performing PPE candidates. Several improvements regarding the testing of submicron particle filtration are progressively better addressed and harmonized with the other PPE filtration efficiency assessments through methods, including the recently modified F2100-23 Standard Specification for Performance of Materials Used in Medical Face Masks.

Yet, gaps remain in the assessment of viable microorganisms such as *S. aureus* (∼1.2 μm), with respirators, not masks, being the appropriate device to protect against exposure to critically important size ranges (2.2 μm and smaller).

Computational modelling of PPE

Interest in examining PPE through statistical or computational modeling expanded during the COVID-19 pandemic. Several prior studies highlighted empirical relationships between fiber thickness, negative space produced through fiber overlap (pores), material fiber packing density, and other physical parameters for masks, respirators, or gowns (Bai et al. 2021; Paul et al. 2020). A recurring theme in these studies was the importance of pore size in BFE from PPE constructed using spunbond and meltblown polypropylene (Avinash Patil et al. 2022; Bai et al. 2021; Nandy et al. 2020; Schwerin et al. 2020). Particles are filtered by fibers by way of diffusive, interceptive, electrostatic, gravitational, inertial, and/or other mechanisms (Bai et al. 2021; Paul et al. 2020; Payet et al. 1992; Schwerin et al. 2020).

Drawing analogous insight from studies on inhalation and deposition patterns in pulmonary tissue, reports indicate that particles 3.0–5.0 μm or larger are subject to inertial deposition, and they typically affect the upper respiratory tract (Rostami 2009). Particles that are 0.5 μm or smaller, including SARS-CoV-2 at ∼ 0.01 μm (or droplet nuclei), experience Brownian diffusion and have random particle motion while also remaining suspended in the air for longer periods (Rostami 2009).

The above-mentioned mechanisms of particle capture in the context of PPE led to the single fiber filtration efficiency (SFFE) equation for modeling respirators (Bai et al. 2021). Notably, SFFE defines the filtration efficiency of one fiber; this metric is then incorporated into the filtration efficiency (OFE) equation for a filter (Bai et al. 2021; Corbin et al. 2021). Multiple mechanisms of deposition may coincide and potentially influence each other depending on environmental parameters, and more than one mechanism may be described to predict the filtration efficiency of fibrous filters (Bai et al. 2021; Corbin et al. 2021).

Importantly, the current filtration efficiency (BFE or OFE) equations do not consider the number of pathogenic particles that penetrate a respiratory protective device as per ASTM F2101-23. Therefore, one objective of this effort was to develop a computational model to assess PPE materials that provides insight into particle filtration across a range of particle sizes as captured through a six-stage cascade impactor (an instrument that models particle deposition along the human bronchus alveoli). This computational model aims to

identify the effectiveness of a given filter material with respect to the concentration of viable particles able to penetrate a respirator, described as a $\log_{10}$ reduction.

Motivation for current work

The standards described above call for a more efficient and, importantly, quantitative experimental performance output. To meet these needs, we describe a computational model that may eventually, in turn, be used to expedite current assessment practices. The approach includes examining the microstructure of surgical N95 respirator barrier materials, employing SEM as outlined by the FDA-recognized standard ASTM F2450-18 **S**tandard Guide for Assessing Microstructure of Polymeric Scaffolds for Use in Tissue-Engineered Medical Products to image fibers and pores, followed by ImageJ analysis (Schindelin et al. 2012). It continues with performance testing of surgical N95 respirators based on test methods described in ASTM F2101-23. The information gathered from the microstructural and performance assessments was then incorporated into a conservative computational model. The advantage of this approach is that it provides a rapid means of estimating the filtration efficiency for viable microorganisms using a GUI to serve as a filtration efficiency calculator. The objectives regarding gown testing included the measurement of microstructures using SEM image analysis of critical zones from material layers, including the assessment of these materials following exposure to chemical treatments used as decontamination modalities during the pandemic.

Methods

Surgical N95 respirators

Four different commercially available surgical N95 respirator products were purchased through Amazon Inc. (amazon.com) and CIAMedical (ciamedical.com). Respirator models were de-identified and classified for testing purposes as R1, R2, R3, and R4. Three manufacturers were used, with R1 and R2 made by the same manufacturer. Due to limited supply, these four specific N95 surgical models were available for testing. In addition to these respirators, a mask was used as a negative control—the mask did not require FDA clearance or NIOSH approval as it is not a regulated product, and the indications of use do not demonstrate product performance as a surgical mask or surgical N95 respirator.

Respirator sample preparation

The sampling process involved cutting 1 cm x 1 cm samples from the top (nasal bridge), middle (nostrils), and bottom (mouth) regions of all respirators, separating the samples into base material layers (i.e., "inside"—layer in contact with skin; "middle"—filter layer; "outside"—layer exposed to the environment). Samples were acquired from the described locations, which are notable points of contact for the user. Samples were loaded onto 12.77-mm flat top SEM stages using double-sided tape, then sputter-coated with 10 nm of gold and imaged at a magnification that was relative to the material layers (i.e., each layer of each respirator was unique to a given product, with magnification for each layer determined based on the dimensions of a given layer; magnification for each layer is provided with SEM image data in the Supplemental Materials section) using the TESCAN Mira 3 scanning electron microscope with a secondary electron detection setting and a beam voltage of 5 kV. Figure 1 provides a schematic description of SEM analysis, along with locations of fabric acquisition from each respirator (including individual layers). ASTM F2450-18 was used for SEM analysis to inform these methods.

Cross-sectional imaging of respirators

Cross-sectional images were taken from all four respirator models to generate a side profile of each layer. These images were analyzed for the width and packing density of fibers in each fabric layer. Data from the filtration layers were incorporated into the computational model. The sampling process involved 1 cm × 0.5 cm samples from the middle (nostrils) region of all respirators, separating the samples into layers, as described in Figure 1 (II). Samples were loaded onto 12.77-mm 90° slant SEM stages using double-sided tape. Imaging was performed on control respirators ($n = 3$ per respirator model). These samples were then sputter-coated using 10 nm of silver and imaged with the TESCAN Mira 3 scanning electron microscope using a secondary electron detection setting and a beam voltage of 5 kV. Silver was used for sputter-coating of these samples due to the degradation of the gold target on these specific samples. The silver did not show a significant effect on image quality and acquisition. From each of the three respirators, five measurements were taken from a cross-sectional image. Cross-sectional thickness was measured in ImageJ. The ellipse function was used to draw a circle such that its diameter reaches both the inner and

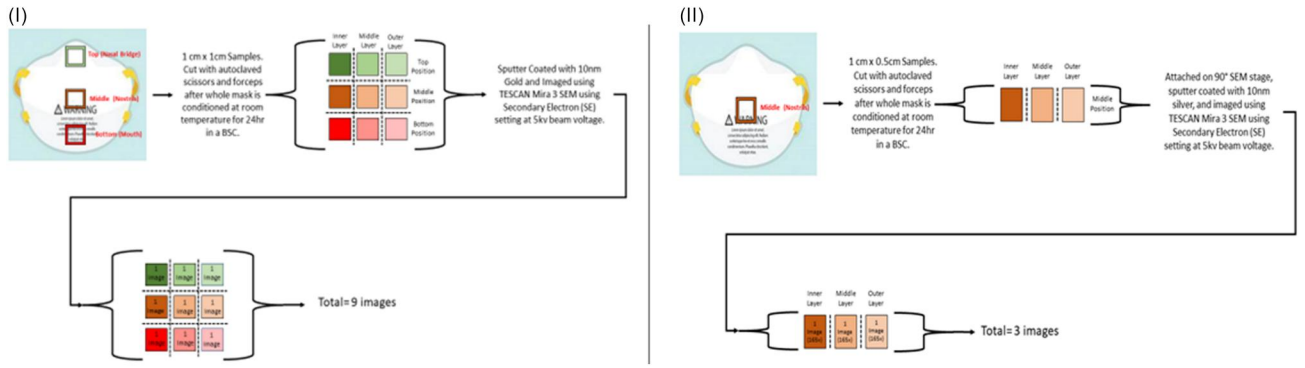

Figure 1. Schematic of standard SEM sampling and imaging process. (I) The schematic shows the R1 respirator as an example of average throughput—four surgical N95 respirator models were examined (R1, R2, R3, R4). Three respirators from each respirator model were tested. From a single respirator sample, nine sections were imaged. Sections for imagining were collected from the following locations: top (nasal bridge); middle (nostrils); bottom (mouth). At each of these locations, three distinct layers were individually imaged. In sum, 27 SEM images were captured from each individual respirator. Importantly, the computational model was informed by the images of the filtration layers ($n = 9$ images per respirator model). (II) Schematic of cross-sectional sampling and imaging process. Described is the typical throughput for three layers from each respirator. Triplicate respirator samples ($n = 3$) were examined per respirator model. Three images were acquired from each respirator, and a total of nine images were acquired from each respirator model. These images provided information on the thickness of each layer. The visual field size of SEM images was 184.84 μm × 158.84 μm (for portrait orientation of SEM images) and 184.84 μm × 126.35 μm (for landscape orientation of SEM images). From each image, five measurements were acquired for thickness, with a detailed description provided in the title, "Cross-Sectional Imaging of Respirators." A more descriptive catalog of magnification used for each layer of respirator (outer, middle, inside) is provided in the Supplemental Material section. The computational model was informed, exclusively, with the images of the filtration layers ($n = 3$ images per respirator model).

outer surface edges of the material. The diameter of the concentric area was recorded as the material thickness.

Analysis of SEM images using ImageJ/Diameter J

Images generated from SEM were modified to 8-bit black-and-white images using ImageJ (Fiji v1.51) for input compatibility into image processing (Hotaling et al. 2015). Using the Diameter J plugin for ImageJ, processed images were subjected to segmentation by way of 16 default algorithms and turned into sets of 8 binary images representing the type of algorithms chosen (Hotaling et al. 2015). Images were segmented using the Diameter J plugin, which provided 16 default algorithms from one SEM image (Hotaling et al. 2015). Diameter J was used again to analyze these binary images for fiber characteristics and further organized, combined, and analyzed to extract an average fiber diameter.

Bacterial filtration efficiency testing

BFE testing of respirators was performed according to ASTM F2101-23. The details of the operating parameters are described in Figure 2, and additional information regarding the instrumental setup is shared in Supplemental Figure 1. Following air sampling, agar plates were incubated at 37 °C for 24–48 h, and colonies were counted to examine the concentration (CFU/ml) of cells that penetrated PPE.

BFE assembly

A ThermoPro TP50 temperature/humidity sensor (Amazon, WA) was used to track temperature within the safety cabinet. Zip ties were used to fasten the laboratory ring stand and the TE-10-800 six-stage viable Andersen cascade impactor (Tisch Environmental, OH) onto a large laboratory retort stand. WANMIN clear car door edge guards (Amazon, WA) were attached to the bottom end of the KETELAMP hurricane glass column with dimensions: 6.35 cm × 25.4 cm (Amazon, WA). Laboratory clamps were used to align and hold the glass column to the opening of the Andersen cascade impactor. Attached to the bottom of the glass column was a concentric silicone ring cutout (outer diameter 7 cm; inner hole diameter 5 cm) from TDHDIKE silicone sheets (Amazon, WA). A glue gun and parafilm were used on the top end of the glass column to attach a 3D printed adaptor with conductive filaments (ProtoPasta, WA). The exit of the collision nebulizer

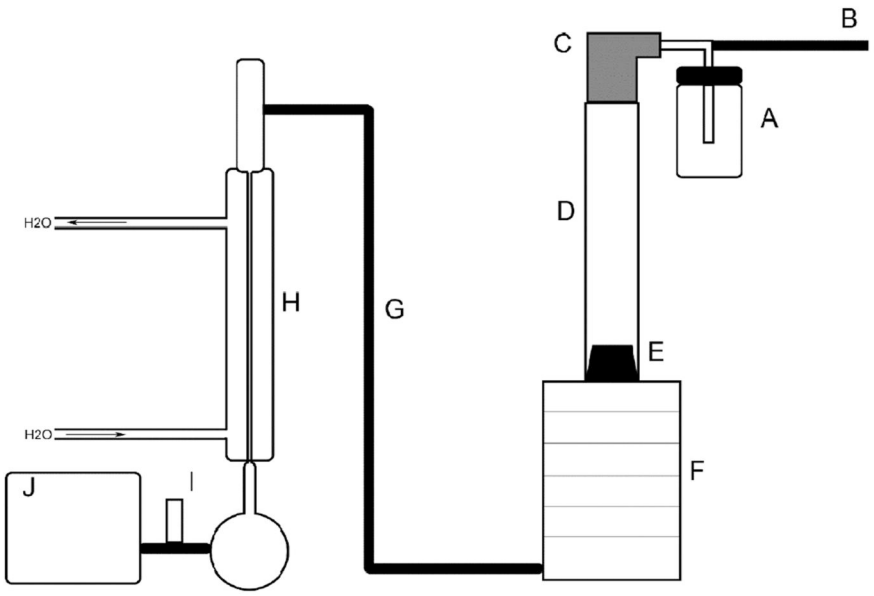

BFE Operating System & Conditions	
Temperature	23 °C
Air Flow Rate	28.3 L/min
Test Organism	*Staphylococcus aureus* (ATCC 43300)
Concentration of Organism	10^5 CFU
Particle Collection System	Six Stage Andersen Air Impactor with Nutrient Agar (NA) Plates

Figure 2. Diagram of bacterial filtration efficiency complex for PPE microbial penetration/filtration testing. A: Collison nebulizer; B: air intake; C: 3D printed elbow joint/adapter; D: glass column; E: rubber stopper/respirator testing site; F: six-stage Andersen cascade Impactor; G: tubing; H: condenser w/flask; I: gas flowmeter; J: compressor. Test conditions are provided in the adjacent table. Further details regarding the assembly, installation, and operation are provided in greater detail with descriptions of the corresponding materials and methods.

unit (BGI Inc, MA) was inserted into the 3D printed adaptor. The nebulizer was held by a clamp and connected to an external house air source with 10 liters per minute. The outlet tubing to the Andersen cascade impactor was then connected to a flask to collect all particles existing in the Andersen cascade impactor. Seventy-percent ethanol was used to disinfect the BFE tower before placing the system into the biosafety cabinet. Aluminum foil was used to ensure that the system was fully grounded.

BFE reservoir installation

Laboratory clamps were used to hold the QWORK Liebig glass condenser (Amazon, WA). EDSRDUS SG01A high-vacuum grease (Amazon, WA) was applied to the connecting end of the glass adaptor before a connection was made from the opening of a Buchner flask (Thermo-Fisher Scientific, MA) to the bottom of the condenser. A clamp was used to secure the Buchner flask to the stand. The opposite opening of the Buchner flask was connected to the inlet of a CNBTR Acrylic LZQ-7 gas flowmeter (Amazon, WA) with Tygon tubing (Lowes, NC). The outlet of the flowmeter was connected to the compressor of the Andersen cascade impactor. The condenser was connected to a sink via Tygon tubing. The outlet tubing connected the Andersen cascade impactor to the inlet of the condenser.

BFE operation

Eight mL of distilled water was added to the reservoir unit. Continuous cold water was supplied to the condenser. Both compressors were monitored to ensure a flow rate of 28.3 L/min. A candle-based smoke test was used to ensure negative pressure at the top of the glass column and the opening of the reservoir. Soapy water was applied around the junctions of the BFE tower and reservoir to ensure no leakages. Bacterial samples were loaded into the Collison nebulizer. Sterile NA plates were loaded into each of the six stages. Each compressor for the Andersen cascade impactor and nebulizer was operated for 60 s. After the completion of a test, Nutrient Agar (NA) plates were incubated, inverted at 37 °C for 48 hr, and inspected for CFU.

Decontamination exposure methods

Ozone treatment of PPE

The ODC used in this study comprised the following components: an air pump, an ozone generator, a nebulizer, and a D16 PortaSens detector (Supplemental Figure 1). Once ozone concentration reached greater than 10 PPM and relative humidity was greater than 80%, the respirators were treated for 90 min (ozone concentrations stabilized approximately 10 min into the decontamination run), at which time the nebulizer and ozone generator were turned off. When the PPM level dropped to less than 0.1 PPM, the respirators were retrieved and placed in a biological safety cabinet overnight. Figure 3 provides an overall layout of the ODC complex.

Vaporized hydrogen peroxide treatment of PPE

Samples were loaded into the hydrogen peroxide decontamination complex (HPDC) (Schwartz et al. 2020). See Figure 3. The fundamental complex was similar to the ODS described above, but with the replacement of the D16 PortaSens ozone sensor with the VHP sensor (Supplemental Figure 3). The HPDC was carefully placed into the secondary container and moved to a certified chemical ventilation hood (Supplemental Figure 3). The VHP sensor was placed within 1 cm of the sample.

When treatment was complete, the nebulizer was shut off. When PPM levels dropped to less than 10 PPM, samples were retrieved and aerated overnight on racks in a Biosafety Level-2 cabinet (BSL2). Figure 3 illustrates the fundamental experimental setup of the HPDC.

Computational modelling methods

The physics-based computational model comprises a set of constitutive equations that depend on measured filter properties. The distribution of these properties are used in a Monte Carlo simulation to provide a distribution of filtration efficiencies. The details of the model, equations, and resulting OFE are provided below, along with a glossary of terminology.

Considered are mechanisms most relevant to the standard protocol that will be described herein for BFE testing, following:

- Interception: particles deviate from the air stream and encounter the fiber surface, effectively removing the particle from the air stream.
- Inertial impaction: particles with greater inertia will not follow the change in flow as air passes through a random assortment of fibers, causing these particles to encounter fibers and become trapped.
- Diffusion: random Brownian motion causes small particles to be captured by the fibers.
- Combinatorial diffusion and interception: A combinatorial mechanism of diffusion and interception for when the effective particle size range of diffusion and interception overlaps, with these mechanisms complementing each other.

The equations mentioned below consider the physical dimensions of the filter fibers, their packing density, the challenge particle to be filtered, and the flow velocity, along with other characteristics of the carrier fluid, as well as concepts such as particle drag.

Variables incorporated into the computational model

To assist with demonstrating mechanisms and equations used in the development of this model, the following is a list of terminology to describe each trait incorporated into the model:

- d_f Fiber diameter: length of a straight line through the center of a cross-section of a fiber (mm)
- α Packing density: describes how tightly packed the fibers are in the respirators (1 − porosity) (unitless)
- L Thickness: distance from the inner-facing side to the outer-facing side of the respirator filter layer (mm)
- η_I Filtration efficiency due to inertial impaction (unitless)
- η_R Filtration efficiency due to interception (unitless)
- η_D Filtration efficiency due to diffusion (unitless)
- η_{DR} Filtration efficiency due to interception and diffusion (unitless)
- η Total SFFE: the combined SFFE of all mechanisms of deposition (unitless)
- E Combination of SFFE with fiber diameter, packing density, and thickness: the filtration efficiency of a fibrous filter material (unitless)
- Stk Stokes number: ratio of characteristic time of a droplet to characteristic time of flow (unitless)
- Cu Cunningham slip factor for a particle in a fluid (unitless)
- ρ_d Particle density (kg/m^3)
- d_p Particle diameter (μm)
- V Face velocity: speed of fluid at the challenge area of the material (m/sec)
- μ Fluid viscosity (N * s/m^2) or (kg/m * sec)

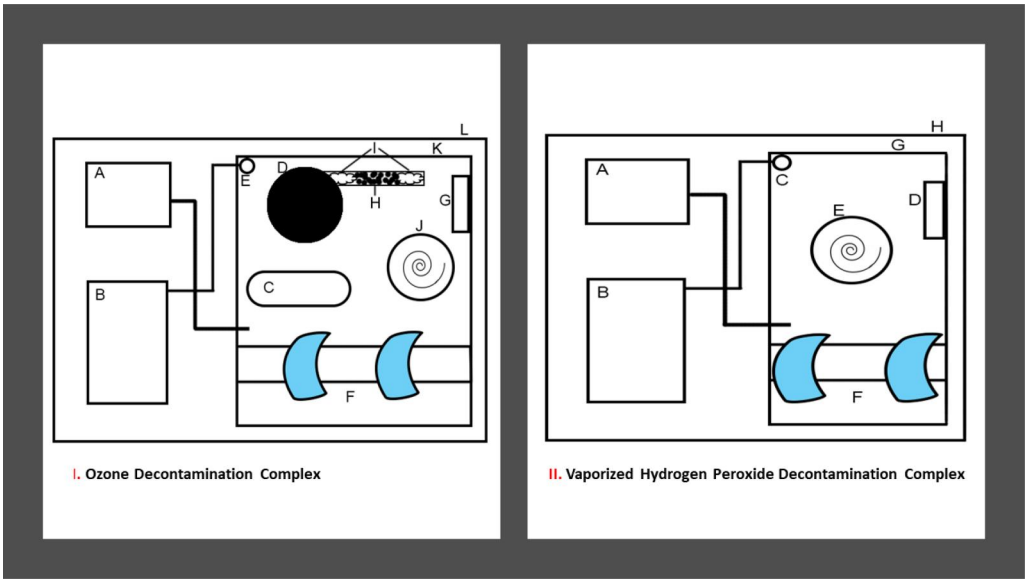

Figure 3. Diagram I—ozone decontamination complex (ODC). Highlighted are the fundamental components of each of the decontamination complexes. The outer container is the secondary containment system, and the inner container is the primary containment system. A: ozone/VHP sensor; B: nebulizer; C: ozone generator; D: air pump; E: nebulizer reservoir; F: respirator samples; G: temperature and humidity sensor; H: Carulite; I: glass wool; J: small fan; K: primary container; L: secondary container. Diagram II—vaporized hydrogen peroxide decontamination complex (HPDC). The fundamental components of the system included the following: in the secondary container (H) (A: VHP sensor (nozzle extends into primary container for readings); B: nebulizer); in the primary containment system (G) (C: nebulizer reservoir D: temperature and humidity sensor E: small fan F: respirators). Multiple detailed images of the ODC and HPDC are provided in the Supplemental Material section to further complement detailed methods.

Pe Péclet number: ratio of the rate of advection to the rate of diffusion (unitless)
Kn Knudsen Number: ratio of the molecular mean free path of gas to the particle or fiber radius (unitless)
k_{Ku} Kuwabara flow field equation: the flow surrounding a fiber (unitless)
C_d Coefficient of correction for diffusion (unitless)
D Diffusion coefficient (m^2/sec)
k Boltzmann constant (N * m/K)
C_n Cunningham slip factor at the fiber surface (unitless)
T Temperature (K)
λ Mean free path of an air molecule (nm)
k_s Kuwabara flow field equation altered by Kirsch and Stechkina (unitless)

Summary of mathematical equations

The following equations were used to describe filtration efficiency attributed to the respective mechanisms of particle deposition:

Overall filtration efficiency (Bai et al. 2021):

$$E = 1 - \exp\left[-\frac{4\eta\alpha L}{\pi d_f(1-\alpha)}\right] \quad (1)$$

Total SFFE (Bai et al. 2021):

$$\eta = \eta_D + \eta_R + \eta_I + \eta_{DR} \quad (2)$$

Diffusion and interception (Stechkina et al. 1969):

$$\eta_{DR} = 1.24\frac{R^{2/3}}{\sqrt{k_s Pe}} \quad (3)$$

$$k_s = -0.5\ln(\alpha) - 0.52 + 0.64\alpha + 1.43(1-\alpha)Kn \quad (4)$$

Diffusion (Payet et al. 1992):

$$\eta_D = 1.6\left(\frac{1-\alpha}{k_{Ku}}\right)^{\frac{1}{3}} Pe^{-\frac{2}{3}}\left(\frac{1+0.388Kn\left(\frac{(1-\alpha)Pe}{k_{Ku}}\right)^{\frac{1}{3}}}{1+(\eta_{D,Liu})}\right) \quad (5)$$

$$\eta_{D,Liu} = 1.6\left(\frac{1-\alpha}{k_{Ku}}\right)^{\frac{1}{3}} Pe^{-\frac{2}{3}} C_d \quad (6)$$

$$C_d = 1 + 0.388Kn\left(\frac{(1-\alpha)Pe}{k_{Ku}}\right)^{\frac{1}{3}} \quad (7)$$

$$Pe = \frac{d_f V}{D} \quad (8)$$

$$D = \frac{kC_n T}{3\pi\mu d_p} \quad (9)$$

$$Kn = \frac{2\lambda}{d_f} \quad (10)$$

Interception (Liu and Rubow 1990):

$$\eta_R = \frac{1-\alpha}{k_{Ku}} \frac{R^2}{(1+R)^{\frac{2}{3}-3\alpha}} \quad (11)$$

$$R = \frac{d_p}{d_f} \quad (12)$$

Impaction (Gougeon 1994):

$$\eta_I = 0.0334 Stk^{3/2} \quad (13)$$

$$Stk = \frac{Cu\rho_p d_p^2 V}{18\mu d_f} \quad (14)$$

Statistical analysis methods and computational model development

The programming languages used were R and Python. R was used for statistical analysis and computational model generation. Python was used for the tool framework and web framework. Code was created using Rstudios v1.1.456 with R v4.2.3 and VS Code v1.91.1 with Python v3.9.13.

The Student's t-test was used to compare the experimental results for viable *S. aureus* (CFU/mL) from each of the six stages of the Andersen cascade impactor and compared with the mean and the distribution from the Monte Carlo simulation (data not shown).

The model was informed by distributions for fiber diameter, packing density, thickness, and particle size based on values obtained thus: (1) fiber diameter, thickness and mean values thereof (+/-SD) were measured from SEM images using Diameter J; (2) Packing density was calculated using the mass per unit area (g/m^2) combined with density of the nonwoven fabric (polypropylene, g/m^3) and the thickness of the layer (m). The sections used were approximately 3.8 cm x 2.5 cm; (3) Particle size ranges at each of the six stages of the Andersen cascade impactor are described as provided in the operational manual (Tisch Environmental, Cleves, OH). Normal distributions were generated using the means and standard deviations; fiber diameter was truncated using the minimum and maximum values from Diameter J, while packing density was truncated to the range of 0.01 to1.0.

Monte Carlo simulation

The parameters were subjected to a Monte Carlo simulation by generating 10,000 replications of each parameter following a truncated normal distribution (Mooney 1997). Ten thousand overall filtration efficiency *(E)* predictions were generated by the Monte Carlo simulation. The 10,000 OFEs were converted into $\log_{10}$ reduction values using the following equation:

$$[-Log_{10}(1-E)] \quad (15)$$

This value has a maximum value corresponding to the limit of detection (LOD) of each respective stage of the cascade impactor:

$$LOD = \left[-Log_{10}\left(\frac{1}{positive\ control}\right)\right]. \quad (16)$$

Log_{10} reduction values were normalized to a value within the range 0-1 by factoring out the total positive control values per stage from experimental data.

Model verification

We verified the model by determining the minimum number of iterations needed to converge the model predictions, starting with 10^1 iterations, and increasing by a factor of 10 up to 10^7. The log reduction in viable *S. aureus* for each Andersen cascade impactor stage was measured at each stage and for each experimental iteration. Log reduction refers to the logarithmic (base 10) decrease in the number of viable *S. aureus* cells at each stage. Values for fiber diameter, packing density, and thickness were set to the mean value of each of the individual respirator models. A standard deviation equal to the mean for parameter distribution was used to represent the worst-case scenario for model accuracy. The criteria for successful verification—results for each stage—are within 0.1 of the next two iterations. The minimum required N to meet this criterion was 10,000 (this is further described in the Monte Carlo Simulation section). Model verification was conducted using R packages tidyr and ggplot2.

Model validation

Models were validated by comparing the normalized log reduction values from modeling and experiments. Validation is confirmed when the experimental values fall within the reported 5th percentile from the model for each stage of the Andersen cascade impactor. Model validation was conducted using R and Microsoft Excel. Normal distributions were generated using the truncnorm package in R.

Model sensitivity

Sensitivity analysis was conducted using the R package ggplot2 to generate contour plots comparing the effects of fiber diameter, thickness, packing density, and particle size on OFE. Six plots were generated to represent the minimum particle size of the six stages of the Andersen cascade impactor. Contour lines

represent the 95% threshold of OFE at four different packing densities. For each respirator model or mask, the fiber diameter and thickness were plotted for comparison to the contour lines (Figure 4).

Results

SEM imaging for surgical N95 respirators

SEM imaging of filter layers reveals fibrous microstructure, as shown in example images of Figures 5 and 6. Analysis by ImageJ yields ranges of values for measurements of fiber diameter, two-dimensional porosity (negative space) from which packing density is calculated, and thickness of the filter layer for each model of respirator. These values are summarized in Table 2. The mean fiber diameters for the surgical N95 respirators fall into a tight range, with the mask demonstrating the smallest mean fiber diameter and the lowest mean packing density (~0.069 µm). Similarly, the mean material thickness in the mask is less than the surgical N95 respirators. R2 has the greatest mean fiber diameter (~5.01 µm) and the highest mean packing density (~0.13 µm). R3 has the lowest material thickness (714.34 µm) and second highest packing density (0.096 µm). The most variable property measured among respirators was thickness, which demonstrated a greater range in standard deviation for surgical N95 respirators compared with the mask.

SEM imaging also allowed examination for measurable changes in the four respirator models and masks due to exposure to decontamination modalities (VHP or ozone). A Student's t-test of two samples assuming equal variances was performed between controls and compared with decontamination modalities. No discernible changes to fiber diameter, thickness, or porosity were identified from samples treated with one or three cycles of ozone when compared with untreated controls. Two respirator models showed a significant difference after exposure to VHP (3x treatment cycles) when compared with the controls for two-dimensional pore size as indicated through Diameter J (R1; ($p \leq 0.043573$ and R4; ($p \leq 0.023273$). More SEM images of respirators are referenced in the Supplemental Material section and located at GitHub: https://github.com/OSEL-DBCMS/PPECalculator.

Bacterial filtration efficiency test and overall filtration efficiency: Comparison of results from experimental and computational models

In this examination of the BFE system, 1×10^3 CFU/ml was tested for the positive control conditions (no respirator). Five biological replicates were tested, and the results showed no significant variation between test runs and no significant difference in the viable concentration of *S. aureus* recovered from nutrient agar (NA) plates from each stage of the Andersen cascade impactor, demonstrating that the conditions of the system were reliable and reproducible (data not shown) (Figure 7).

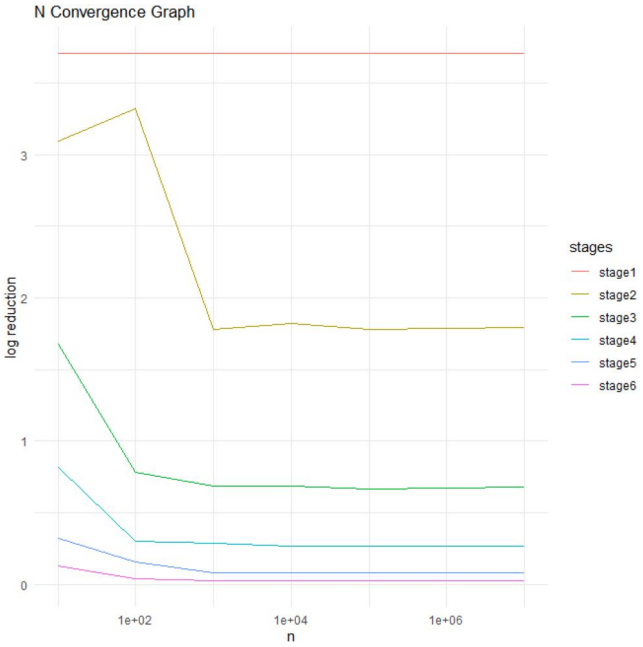

Figure 4. Verification plot (N convergence graph). Log reduction values were measured relative to the number of replications. The mean for fiber diameter was set at 4 µm, and the standard deviation was also set at 4 µm. Packing density was set at a mean of 0.1 µm (S.D. ± 0.1 µm). The mean for thickness was specified to 1,000 µm (S.D. ± 1,000 µm). Minimum values were predetermined for each parameter such that negative values were not included. For the x-axis, N = number of simulations, and the y-axis shows $\log_{10}$ reduction in filtration. Each stage (1–6) represents a particle size range of the Andersen cascade impactor.

After completing validation of the BFE system as previously described, all four respirator models and one mask were tested with triplicate biological samples ($n = 3$), and BFE was calculated for each respirator model using the equation provided in ASTM F2101-23. Results for all four respirator models demonstrated BFEs above 95%, including the mask. The results of this study were further examined relative to the Andersen cascade impactor stages (1–6) and for decontaminated samples. Results from samples examined from all six stages of the Andersen cascade impactor showed a statistically significant difference in microbial penetration observed at stage 6 for respirators R1, R4, and the mask. Additionally, a

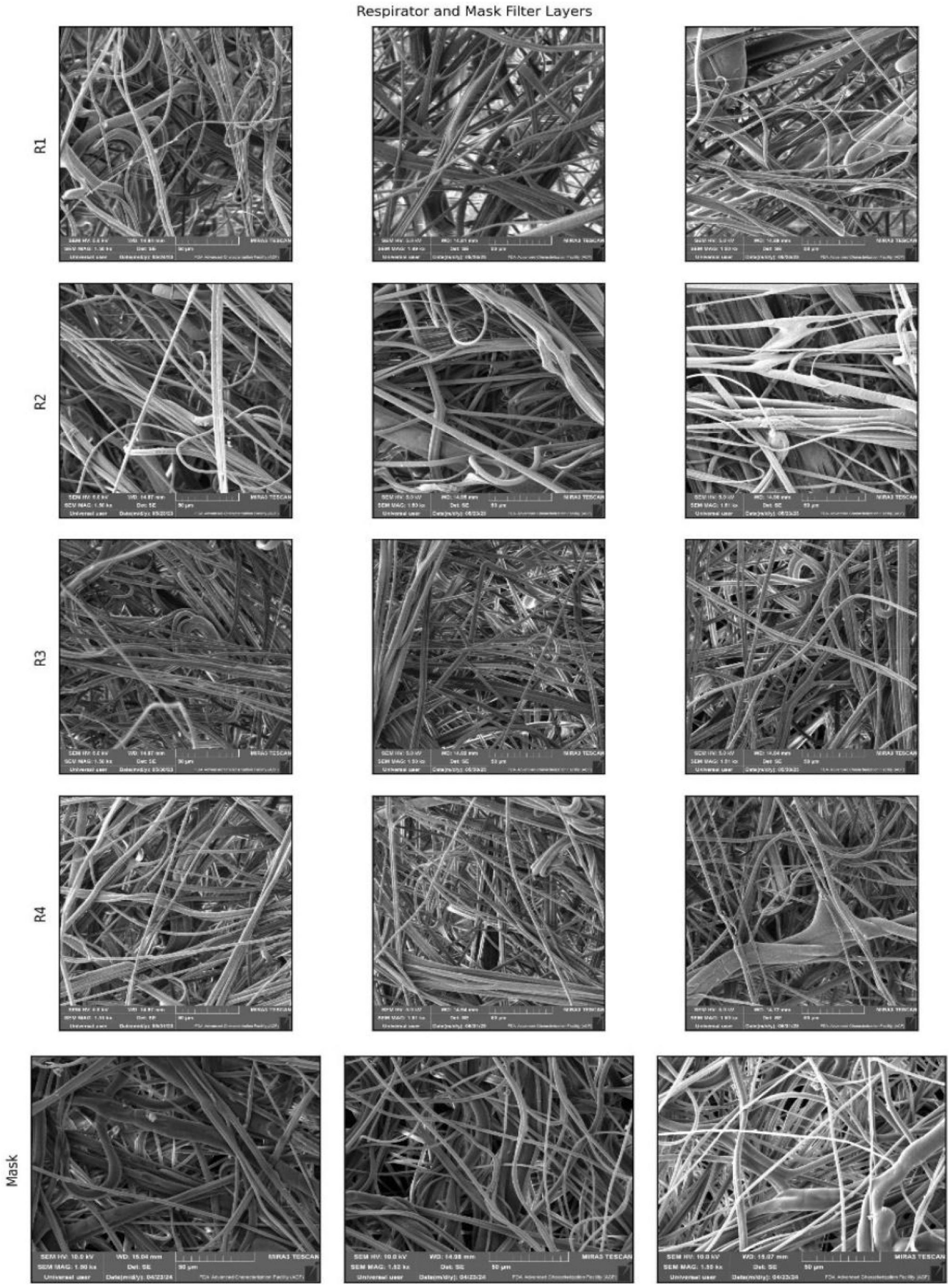

Figure 5. Surgical N95 respirators and mask filter layers. Provided are three images for each filter layer from the four respirator models and the mask. Images of this quality and magnification (1.5kx for respirators and 1.41kx for masks) were analyzed for each of the parameters incorporated into the computational model.

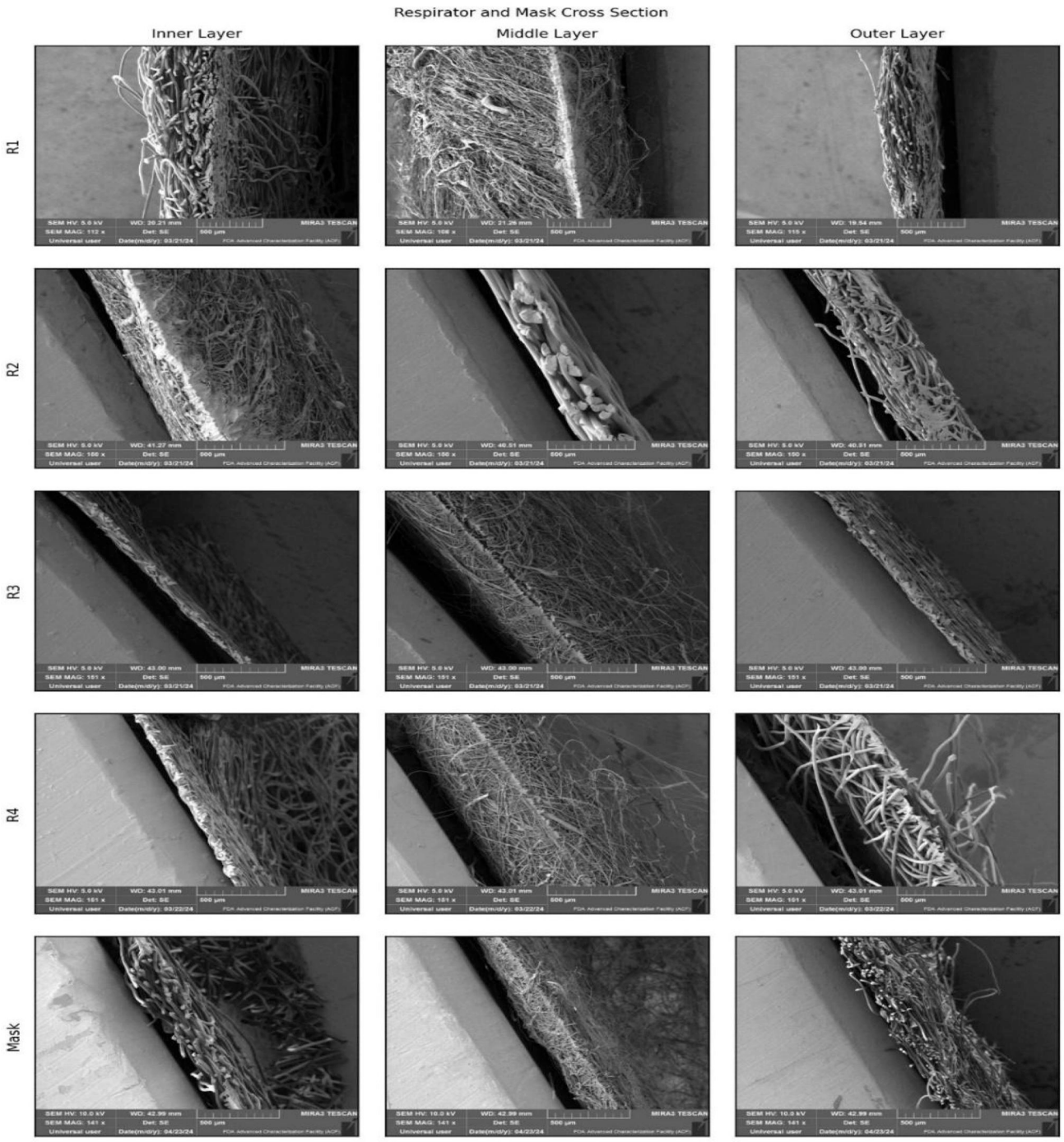

Figure 6. Cross-section of respirators and mask filter layers. Provided are cross-sectional images of each of the three layers that compose a single respirator. Displayed are the four respirator models tested in this study. The middle image in each row is the filter layer. Cross-section magnification was variable and relative to the respirator (R1 112x; R2–R4 150x; Mask 141x).

Table 2. Quantitative traits captured through SEM from filtration layers of surgical N95 masks.

Sample	Mean Fiber Diameter (μm)	Mean Thickness (μm)	Mean Packing Density (μm)
R1	4.88 ± 0.32	1628.37 ± 84.97	0.082 ± 0.0038
R2	5.01 ± 0.48	955.99 ± 118.62	0.13 ± 0.0061
R3	4.52 ± 0.32	714.34 ± 53.62	0.096 ± 0.0044
R4	4.36 ± 0.43	1008.59 ± 155.83	0.084 ± 0.0044
Mask	3.12 ± 0.61	374.90 ± 9.25	0.069 ± 0.0043

Fiber diameter and mean fiber thickness were identified from SEM images, with packing density calculated from these parameters.
Parameters incorporated into the computational model.

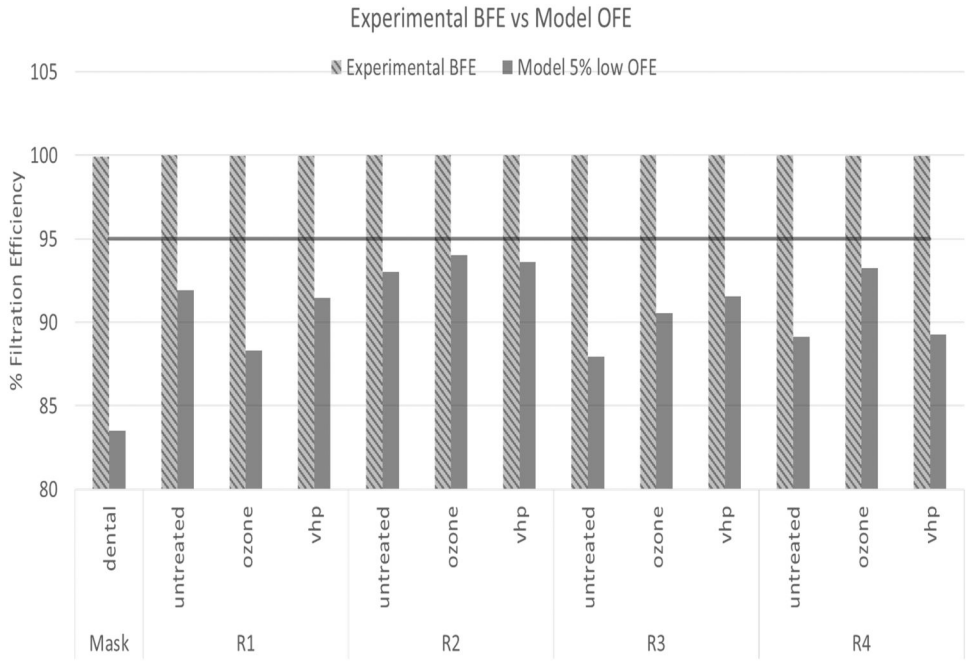

Figure 7. Comparison of BFE from experimental versus the 5th percentile OFE output from the computational model for each respirator model and one mask. BFE and OFE were calculated for respirators that were subject to three cycles of decontamination by ozone and VHP. The horizontal line indicates the 95% threshold. The x-axis describes the experimental conditions, and the y-axis shows the percentage filtration efficiency. From the model, R2 had the highest predicted OFE for untreated samples, followed by R1, R4, and R3, respectively. The least efficient product was the mask.

statistically significant difference was observed for VHP, or ozone-treated samples (included were R1, R2, R3, and R4). However, OFE was above 95% for the mask and surgical N95 respirators for all the experimental conditions tested and controls, per calculations performed with ASTM F2101-23 (data not shown).

Illustrated in Figure 8 are the $\log_{10}$ reduction of viable particles for normalized data; compared are the experimental minima versus the 5th percentile of the model predictions for controls (Figure 8, 1), ozone-treated (Figure 8, II), and VHP-treated (Figure 8, III) samples of each surgical N95 respirator. The trend for $\log_{10}$ reduction from the model shows higher sensitivity than in the experimental data. However, the model complements the experimental data with respect to the penetration of particles in the smallest size ranges, demonstrating less efficiency. It should be noted that the model is more conservative in the predicted log reduction compared with the experimental outcome.

Experimental results for untreated samples show that the greatest log reductions occurred with R2 and R3 respirators. R1 demonstrates a smaller log reduction for particles at the smallest particle size ranges (i.e., Stages 4 and 5, corresponding to 2.2 μm–0.65 μm), while R4 showed a notable reduction at Stage 6 (1.1 μm–0.65 μm). The 5th percentile normalized log reduction predictions fall below their respective minimal experimental value as the particle size decreases, indicating that the model is conservative. Stages 5 and 6 had the smallest calculated log reduction across all the respirators, with R1 and R2 performing better compared with R3 and R4. Similar trends for experimental results and model predictions were observed for ozone- and VHP-treated respirators.

Model sensitivity

Model sensitivity was determined by comparing four parameters: fiber diameter, filter thickness, particle size, and material packing density. Specific values were maintained as constants: (1) the particle size ranges (per comparison to Andersen cascade impactor stages 1–6) and (2) the packing density, respective of each of the respirator models and mask. The fiber diameter and filter layer thickness were varied to examine their effect on OFE.

The combination of all four parameters was used to generate a table of corresponding overall filtration efficiencies as contour plots (Figure 9). As seen in Figure 9, the contour lines represent the 95% threshold for each respective packing density that corresponds to a given respirator or mask. Overall, OFE decreases as the graph shifts to the right and increases as it shifts upward. The points indicate the

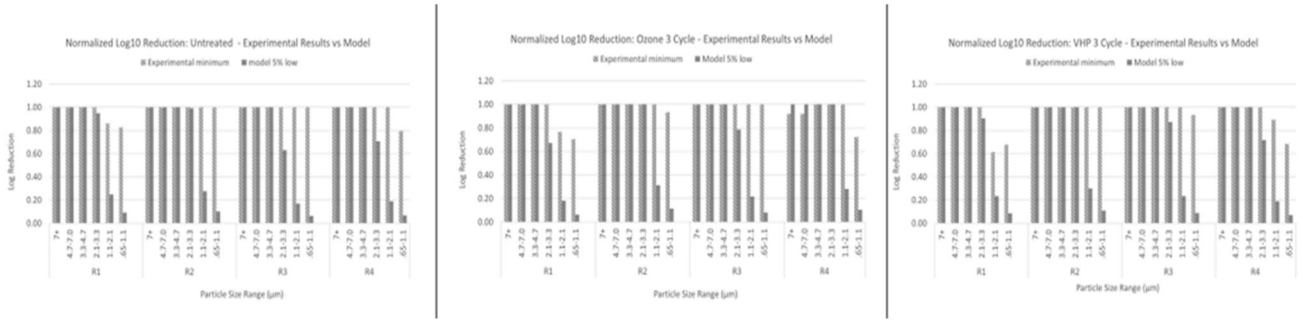

Figure 8. (I) Untreated (control) surgical N95 respirators. Comparison of normalized log reduction values for BFE from experimental minima versus the 5th percentile normalized log reduction values for OFE from the computational model. The x-axis describes the particle size ranges captured at each stage of the Andersen cascade impactor and the performance of respirators (R1–R4). The Y-axis shows the log reduction in filtration of *S. aureus*-bearing particles. The experimental and computational results show minimal difference at particle sizes 7 µm–2.2 μm. At particle sizes 2.2 μm and below, the model shows less efficiency than the experimental values, and the model is therefore conservative. (II) Ozone-treated respirators. This graph illustrates the comparison of normalized log reduction values for BFE from experimental minima versus the 5th percentile normalized log reduction values for OFE derived from the computational model. Comparable to observations made at particle sizes at 2.2 μm and below for controls, the computational model of ozone treated R1 and R4 respirators show lower filtration efficiency than in the experimental results, and all of the respirators perform below the expected 95% in the conservative computational model. (III) VHP-treated respirators. Comparison of normalized log reduction values for BFE from experimental minima versus the 5th percentile normalized log reduction values for OFE from the computational model. Similar to results observed for untreated controls and ozone-treated respirators, VHP-treated respirators demonstrate less filtration efficiency when tested for viable particles 2.2 μm and smaller.

respective fiber diameter and thickness for each product, and the ellipses represent the standard deviation of the means for the two parameters. The colors correspond to a value closest to the respirator's packing density. Additionally, the values that are to the left of each contour line demonstrate filtration efficiency per corresponding respirator. This change then indicates whether the respirator performs within the 95% threshold or deviates outside of this range.

Incorporation of the model into the GUI

The model, coded in R, was translated into Python and compiled into a web hosting service. Accompanying information for the use of the calculator is housed in GitHub (https://github.com/OSEL-DBCMS/PPECalculator). The GUI for the tool can be seen in Figure 10. Users can enter measurements of fiber diameter (d_f), packing density (α), and thickness (L), and insert the mean and standard deviations in the respective input boxes.' from the user's inputs result in these outputs: the normalized $\log_{10}$ reduction values, the 5th, 25th, 50th, 75th, and 95th percentile as graphical and tabular results (see Figure 10).

Discussion

Notable observations from this study included the following: First, decreasing the droplet size from 3.0 µm to a median particle size of ~2.1 µm in BFE tests generated penetration at the submicron particle range. Secondly, ASTM F2101-23 requires a droplet size of 3.0 µm (S.D. 0.1 µm); this particle size, however not effective for testing surgical N95 respirators, as it is currently recommended. The current results show experimental and modeled data indicate testing with a smaller particle size would provide critical penetration; this particle range does not apply to respirator FE tests. Thirdly, calculating overall filtration efficiency as described in ASTM F2101-23 for respirator testing may overestimate product effectiveness at particle sizes that are below 3.0 µM (S.D. 0.1 µm), the median viable particle size recommended by this standard for mask and respirator testing.

Limitations

This conservative computational model provides unique insight into conditions resulting in microbial penetration for materials used in respiratory protection devices. As indicated, these products pass filtration efficiency tests and demonstrate filtration efficiency above 95% according to standard protocols. However, upon closer examination for particle size ranges of 2.2 µm and below, penetration was statistically significant between experimental and modeled results. The focus of this computational model was on the filtration layer of surgical N95 barrier material. This model was optimized for the filtration layer; other layers were not assessed.

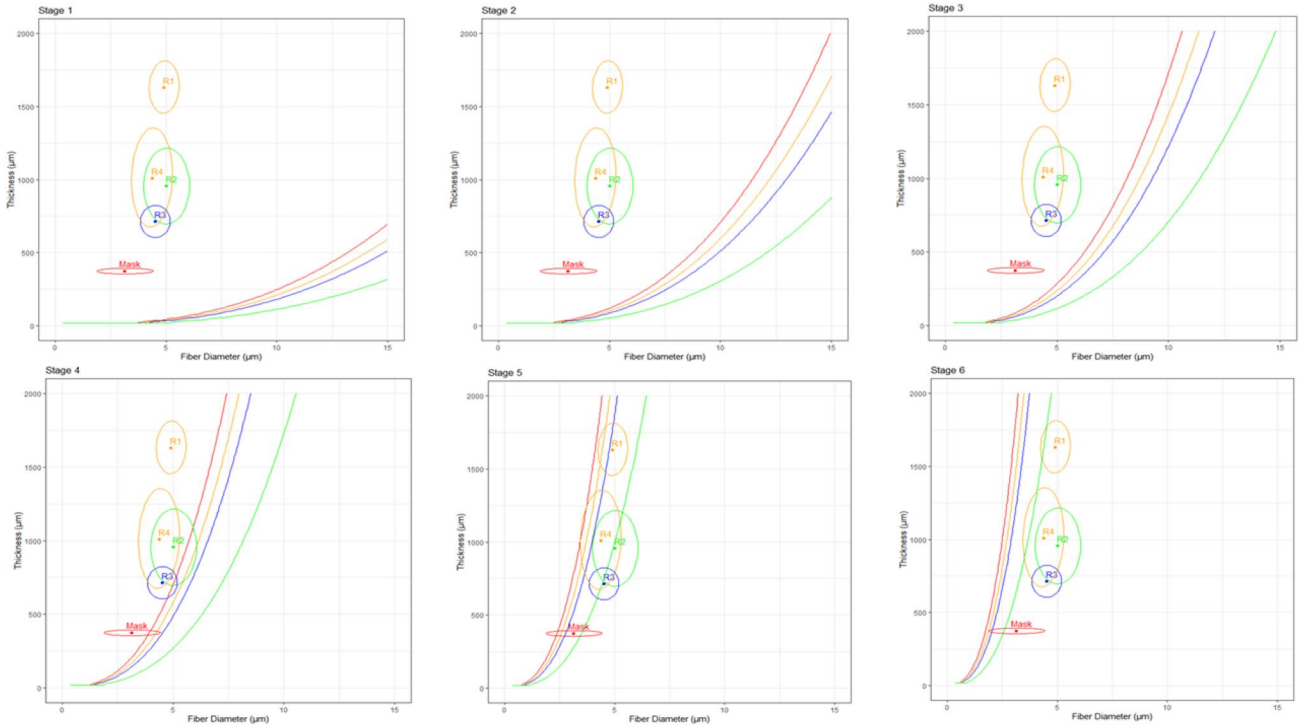

Figure 9. Model sensitivity contour plots. Each plot corresponds to a particle size range captured by each of the Andersen cascade impactor Stages (1–6). The x-axis describes the fiber diameter, and the y-axis describes filter thickness. The contour lines represent the 95% threshold for the packing density values of 0.07, 0.08, 0.09, and 0.13 (left to right). The points represent the average fiber diameter and thickness for each respirator model and the mask. The colors represent each respirator and correspond to a packing density of a given respirator model—as such, "mask" is indicated as a red dot with the ellipse showing the 95% confidence interval, and the red line indicates the corresponding packing density. Mask = red; R1 & R4 = orange; R2 = green; R3 = blue.

Conclusions

A goal of this study was to provide PPE stakeholders with a computational model/tool to inform and expedite decision-making in ideation, design, and manufacturing. The SARS-CoV-2 pandemic exposed PPE supply chain vulnerabilities, notably with N95 respirators and surgical gowns. This study presents a conservative, uniquely SEM informed, physics-based computational model with a user-friendly GUI to assess the filtration efficiency of the respirator filter layers based on material thickness, fiber diameter, and packing density. TEB-APR-STP-0059, ASTM F2100-23, and ASTM F2101-23 remain the standard for filtration testing and are important to biologically relevant evaluation of filter materials. Accordingly, this study evidences (1) the value of viable microbial particle testing along with other physical test methods and (2) approaches to incorporate these data into computational models to build less labor-intensive technology with biologically relevant evaluation of new and decontaminated PPE materials.

Computational modeling and similar tools expedite product evaluation for emergency preparedness (Bai et al. 2021; Corbin et al. 2021; Zhang et al. 2024). This model could be expanded to test latex beads or other submicron particles to assess the efficacy of the model, stratify its use, and expand the functions of the tool to examine filtration efficiency using computational methods.

An objective of the study described herein was to develop an approach to analyze PPE fiber structure via physical testing in conjunction with a physics-based mass transport computational model for the purposes of obviating labor-intensive testing. Although testing for validation would likely always be required, this could be a useful tool at the R&D (material selection) stage or during PPE shortages (as experienced during the COVID-19 pandemic). Specifically, the model may be leveraged to interpret the penetration of a broad range of particle sizes (notably, microorganisms) that can impact the lower bronchoalveolar tissues of the lung. The model might also be used to help probe additive effects of decontamination modalities and mechanical stresses/strain on PPE characteristics, as highlighted by the characterization of Level 3 and 4 surgical gowns (see Supplemental Tables 4 and 5). These findings are of relevance in discussions and decisions around the

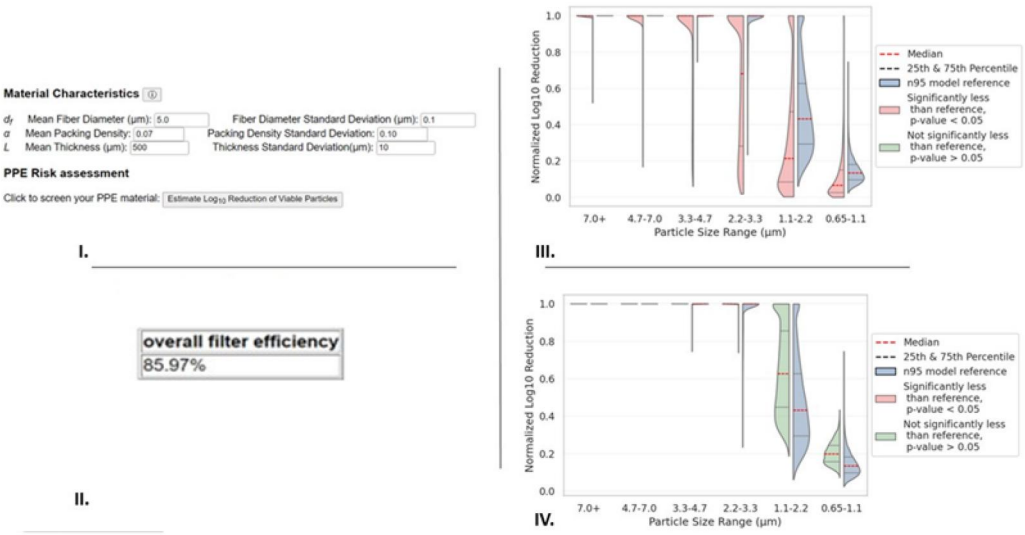

Percentiles of normalized $\log_{10}$ reduction values at each particle size range

Stage	Particle Size Range (μm)	Normalized Log Reduction Value 5th percentile	Normalized Log Reduction Value 25th percentile	Normalized Log Reduction Value 50th percentile	Normalized Log Reduction Value 75th percentile	Normalized Log Reduction Value 95th percentile
1	7.0+	1.000000	1.000000	1.000000	1.000000	1.000000
2	4.7-7.0	0.584631	1.000000	1.000000	1.000000	1.000000
3	3.3-4.7	0.207545	0.746714	1.000000	1.000000	1.000000
4	2.2-3.3	0.075354	0.283999	0.681863	1.000000	1.000000
5	1.1-2.2	0.020366	0.084980	0.215362	0.473789	1.000000
6	0.65-1.1	0.005648	0.026493	0.067949	0.151226	0.418469

Figure 10. PPE Risk Calculator GUI. (I) The input parameters are material characteristics. (II) a table display outputs that included the following information: user inputs OFE of the test subject. (III and IV) Graphical outputs display the performance of a material compared with a reference surgical N95 at different particle size ranges; if the outcome of the user's product performs significantly less than the reference, the "violin plot" is red, but if the output is comparable or better than the reference, the output is green. Additional characteristics detailed in the plot include the mean, distribution density, and $\log_{10}$ reduction at the 25th and 75th percentiles. The bottom table summarizes the normalized $\log_{10}$ reduction output per particle size range for the 5th, 25th, 50th, 75th, and 95th percentiles. In sum, this tool allows the user to examine materials and compare performance with a reference surgical N95 and estimate filtration efficiency. The data that support the findings of this study are available at: https://github.com/OSEL-DBCMS/PPECalculator.

demand, sustainability, and environmental impact of a PPE supply chain (Cubas et al. 2023; Gunasekaran et al. 2022; Lendvay et al. 2022).

Acknowledgments

The authors would like to thank the FDA Office of the Chief Scientist (OCS) Medical Counter Measures Initiative (MCMi), the CDRH Office of Science and Technology (OST), Office of Counter Terrorism and Emerging Threats (OCET). OSEL/DBCMS, and the OSEL Emergency Preparedness Program (Dorn Carranza/Jenna Osborn) for funding and supporting this project. We also thank the ORISE fellowship program for administering support to Sang Hyuk Lee, Thomas Glover, William Kastor, and Andrew Martin. Additionally, we would like to thank Tracy Ulderich (OST/CDRH), Hainsworth Shin (CDRH), David Simon (CDRH), Yi Wang (CBER), Daniel Tadesse (CVM), Tanmay Jain (CDRH), Anne Lucas (CDRH), Advanced Manufacturing Lab (CDRH), and Srilekha Das (CDRH) for their invaluable scientific insights. We would like to thank the following institutions for their contributions and assistance towards this project: Johns Hopkins University Whiting School of Engineering, George Washington University School of Engineering (Dr. Michael Keidar and Dr. Vikas Soni), CDC-NIOSH-NPPTL (colleagues and laboratories for conducting multiple experiments to test respirators and gowns for this project).

Attribution

N95 is a certification mark of the U.S. Department of Health and Human Services (HHS) registered in the United States and several international jurisdictions.

Disclaimer

The findings and conclusions in this manuscript have not been formally disseminated by the Food and Drug Administration (FDA) and should not be construed to represent any agency determination/policy. The mention of commercial products, their sources, or their use in connection with material reported herein is not to be construed as either an actual or an implied endorsement. The findings and conclusions in this report are those of the authors and do not necessarily represent the official position of the National Institute for Occupational Safety and Health (NIOSH) or the Centers for Disease Control and Prevention (CDC). Mention of any company or product does not constitute endorsement by NIOSH, CDC.

Disclosure statement

No potential conflict of interest was reported by the author(s).

Data availability statement

The data that support the findings of this study, including supplemental data (SEM images of respirators and gowns), are available at GitHub: https://github.com/OSEL-DBCMS/PPECalculator. Source code for the web interface is available and will be deployed at a later date. This code can be made available upon request.

References

Adanur S, Jayswal A. 2022. Filtration mechanisms and manufacturing methods of face masks: an overview. J Ind Text. 51(3_suppl):3683S–3717S. doi: 10.1177/1528083720980169.

ANSI/AAMI. 2012. Liquid barrier performance and classification of protective apparel and drapes intended for use in healthcare facilities. Arlington (VA): Association for the Advancement of Medical Instrumentation.

Avinash Patil N, Macchindra Gore P, Shanmugrajan D, Patil H, Kudav M, Kandasubramanian B. 2022. Functionalized non-woven surfaces for combating the spread of the COVID-19 pandemic. Interface Focus. 12(1):20210040. doi: 10.1098/rsfs.2021.0040.

Bai H, Qian X, Fan J, Shi Y, Duo Y, Guo C, Wang X. 2021. Theoretical model of single fiber efficiency and the effect of microstructure on fibrous filtration performance: a review. Ind Eng Chem Res. 60(1):3–36. doi: 10.1021/acs.iecr.0c04400.

Chaib F. 2020. Shortage of personal protective equipment endangering health workers worldwide. World Health Organization. https://www.who.int/news/item/03-03-2020-shortage-of-personal-protective-equipment-endangering-health-workers-worldwide.

Check R, Kelly B, McMahon K, Balakrishnan V, Rivard L, Pester J, Jeanmonod D, Jeanmonod RK. 2021. Failure rates during reuse of disposable N95 masks in clinical practice in the emergency department. West J Emerg Med. 22(3):547–551. doi: 10.5811/westjem.2021.1.49960.

Cohen J, Rodgers YVM. 2020. Contributing factors to personal protective equipment shortages during the COVID-19 pandemic. Prev Med. 141:106263. doi: 10.1016/j.ypmed.2020.106263.

Corbin JC, Smallwood GJ, Leroux ID, Norooz Oliaee J, Liu F, Sipkens TA, Green RG, Murnaghan NF, Koukoulas T, Lobo P. 2021. Systematic experimental comparison of particle filtration efficiency test methods for commercial respirators and face masks. Sci Rep. 11(1):21979. doi: 10.1038/s41598-021-01265-8.

Cubas ALV, Moecke EHS, Provin AP, Dutra ARA, Machado MM, Gouveia IC. 2023. The impacts of plastic waste from personal protective equipment used during the COVID-19 pandemic. Polymers (Basel). 15(15):3151. doi: 10.3390/polym15153151.

Dolez PI, Marsha S, McQueen RH. 2022. Fibers and textiles for personal protective equipment: review of recent progress and perspectives on future developments. Textiles. 2(2):349–381. doi: 10.3390/textiles2020020.

Gougeon R. 1994. Liquid aerosol filtration by fibrous filters in interception and inertial regimes. https://inis.iaea.org/records/pqhn6-26t42

Gunasekaran K, Mghili B, Saravanakumar A. 2022. Personal protective equipment (PPE) pollution driven by the COVID-19 pandemic in coastal environment, Southeast Coast of India. Mar Pollut Bull. 180:113769. doi: 10.1016/j.marpolbul.2022.113769.

Hotaling NA, Bharti K, Kriel H, Simon CG, Jr. 2015. DiameterJ: a validated open source nanofiber diameter measurement tool. Biomaterials. 61:327–338. doi: 10.1016/j.biomaterials.2015.05.015.

Hu B, Guo H, Zhou P, Shi ZL. 2021. Characteristics of SARS-CoV-2 and COVID-19. Nat Rev Microbiol. 19(3):141–154. doi: 10.1038/s41579-020-00459-7.

Jefferson T, Del Mar C, Dooley L, Ferroni E, Al-Ansary LA, Bawazeer GA, van Driel ML, Foxlee R, Rivetti A. 2009. Physical interventions to interrupt or reduce the spread of respiratory viruses: systematic review. BMJ. 339(sep21 1):b3675. doi: 10.1136/bmj.b3675.

Lawrence RB, Duling MG, Calvert CA, Coffey CC. 2006. Comparison of performance of three different types of respiratory protection devices. J Occup Environ Hyg. 3(9):465–474. doi: 10.1080/15459620600829211.

Lendvay TS, Chen J, Harcourt BH, Scholte FEM, Lin YL, Kilinc-Balci FS, Lamb MM, Homdayjanakul K, Cui Y, Price A, et al. 2022. Addressing personal protective equipment (PPE) decontamination: methylene blue and light inactivates severe acute respiratory coronavirus virus 2 (SARS-CoV-2) on N95 respirators and medical masks with maintenance of integrity and fit. Infect Control Hosp Epidemiol. 43(7):876–885. doi: 10.1017/ice.2021.230.

Lin BK, Munter B, Pascavis K, Nakaji P, Nicolasora N. 2021. Use of industrial filters by health care workers during shortages of N95 respirators in pandemic times. Infect Dis Clin Pract (Baltim Md). 29(5):e278–e281. doi: 10.1097/IPC.0000000000001059.

Liu BYH, Rubow KL, editors. 1990. Efficiency, pressure drop and figure of merit of high efficiency fibrous and membrane filter media. Proceedings of the 5th World Filtration Congress; June 5-8 1990; Nice.

Lou L, Chen K, Fan J. 2021. Advanced materials for personal thermal and moisture management of health care workers wearing PPE. Mater Sci Eng R Rep. 146:100639. doi: 10.1016/j.mser.2021.100639.

Masandawa L, Mirau SS, Mbalawata IS. 2021. Mathematical modeling of COVID-19 transmission dynamics between healthcare workers and community. Results Phys. 29:104731. doi: 10.1016/j.rinp.2021.104731.

Mooney C. 1997. Monte Carlo simulation. [accessed 2024 Sep 20]. https://methods.sagepub.com/book/monte-carlo-simulation.

Nandy P, Zhu C, Young M, Wood SC, Lucas AD. 2020. Research: comparing ASTM F1671 with a modified dot-blot method to evaluate personal protective materials. Biomed Instrum Technol. 54(2):102–109. doi: 10.2345/0899-8205-54.2.102.

National Institute for Occupational Safety and Health SB. 2020. Respiratory protection during outbreaks: respirators

versus surgical mask [accessed 2020]. https://blogs.cdc.gov/niosh-science-blog/2020/04/09/masks-v-respirators/.

Paul D, Gupta A, Maurya AK. 2020. Exploring options for reprocessing of N95 filtering facepiece respirators (N95-FFRs) amidst COVID-19 pandemic: a systematic review. PLoS One. 15(11):e0242474. doi: 10.1371/journal.pone.0242474.

Payet S, Boulaud D, Madelaine G, Renoux A. 1992. Penetration and pressure drop of a HEPA filter during loading with submicron liquid particles. J Aerosol Sci. 23(7):723–735. doi: 10.1016/0021-8502(92)90039-X.

Rahman MZ, Hoque ME, Alam MR, Rouf MA, Khan SI, Xu H, Ramakrishna S. 2022. Face masks to combat coronavirus (COVID-19)-processing, roles, requirements, efficacy, risk and sustainability. Polymers. 14(7):1296. doi: 10.3390/polym14071296.

Rostami AA. 2009. Computational modeling of aerosol deposition in respiratory tract: a review. Inhal Toxicol. 21(4):262–290. doi: 10.1080/08958370802448987.

Schindelin J, Arganda-Carreras I, Frise E, Kaynig V, Longair M, Pietzsch T, Preibisch S, Rueden C, Saalfeld S, Schmid B, et al. 2012. Fiji: an open-source platform for biological-image analysis. Nat Methods. 9(7):676–682. English.

Schwartz A, Stiegel M, Greeson N, Vogel A, Thomann W, Brown M, Sempowski GD, Alderman TS, Condreay JP, Burch J, et al. 2020. Decontamination and reuse of N95 respirators with hydrogen peroxide vapor to address worldwide personal protective equipment (PPE) shortages during the SARS-CoV-2 (COVID-19) pandemic. Appl Biosaf. 25(2):67–70. doi: 10.1177/1535676020919932.

Schwerin MR, Portnoff L, Furlong J, Das SS, Gordon EA, Woods TO, Wood SC, Lucas AD. 2020. Evaluation of apparatus used to test liquid through protective materials: comparison of a modified Dot-Blot Apparatus to the ASTM penetration cell. Journal of Testing and Evaluation. 48(1):p. 368–379. English.

Stechkina IB, Kirsch AA, Fuchs NA. 1969. Studies on fibrous aerosol filters. IV. Calculation of aerosol deposition in model filters in the range of maximum penetration. Ann Occup Hyg. 12(1):1–8. doi: 10.1093/annhyg/12.1.1.

World Health Organization. 2021. Worldometer. COVID-19: coronavirus pandemic. https://www.worldometers.info/coronavirus/country/us/.

Zhang L, Alshaikh MK, Lekakou C. 2024. Assessment and design of filters and masks against COVID-19 via modeling and simulations. J Occup Environ Hyg. 21(8):576–590. doi: 10.1080/15459624.2024.2357089.